PHILOSOPHICAL TRANSACTIONS OF THE ROYAL SOCIETY A MATHEMATICAL, PHYSICAL & ENGINEERING SCIENCES

A Review of the Central Role of Nonlinear Interactions in Wind-Wave Evolution

I. R. Young and G. Ph. Van Vledder

Phil. Trans. R. Soc. Lond. A 1993 **342**, 505-524
doi: 10.1098/rsta.1993.0030

A review of the central role of nonlinear interactions in wind–wave evolution

By I. R. Young[1] and G. Ph. Van Vledder[2]

[1]*Department of Civil and Maritime Engineering, University College, University of New South Wales, Canberra ACT2600, Australia*

[2]*Delft Hydraulics, P.O. Box 152, 8300 AD Emmeloord, The Netherlands*

Nonlinear wave–wave interactions play a central role in the development of wind-generated surface waves. A detailed review of computational techniques which have been proposed for their evaluation is provided. Numerical experiments are used to determine the manner in which the nonlinear terms control spectral development with fetch, the directional spread of the spectrum and the high-frequency spectral tail. In addition, the nonlinear terms have a shape-stabilizing role, continually smoothing local perturbations in the spectrum and forcing it back to a 'preferred' shape.

1. Introduction

Following the initial pioneering theoretical work of Hasselmann (1962, 1963*a*, *b*) and the subsequent experimental confirmation during JONSWAP (Hasselmann *et al.* 1973), the important role played by nonlinear third-order resonant interactions in the evolution of wind-wave spectrum has been clearly demonstrated. Numerical evaluation of these interactions, however, poses considerable problems, and solution techniques are computationally expensive. Hence, considerable effort has been devoted to the search for efficient solution algorithms. These computational difficulties, coupled with the inherently complex nature of such nonlinear processes, hinder a complete understanding for many. This paper is intended to provide both an historical review of computational techniques proposed to evaluate nonlinear interactions as well as examples of many of the properties of such interactions. As will be demonstrated, these properties are central to the development of the wind-wave spectrum. An excellent review of the nonlinear theory itself has been presented by Phillips (1981).

As the development in our understanding of nonlinear interactions is inextricably linked to the development of wave prediction models, it is prudent also to review briefly the development of such models.

In the absence of currents, the evolution of the wave spectrum can be described by the energy transfer equation (Gelci *et al.* 1957; Hasselmann 1960; Willebrand 1975), which for deep water is

$$\partial F/\partial t + \boldsymbol{C}_{\mathrm{g}} \cdot \nabla F = S_{\mathrm{tot}}, \tag{1.1}$$

where $F = F(\boldsymbol{k}; \boldsymbol{x}, t)$ is the two-dimensional wavenumber spectrum. Equation (1.1) describes the evolution of the spectrum, components of which are advected at their respective group velocity $\boldsymbol{C}_{\mathrm{g}}$. The source term S_{tot} represents all processes which

Phil. Trans. R. Soc. Lond. A (1993) **342**, 505–524
Printed in Great Britain

transfer energy to or from spectral components. It may be written in the form (Hasselmann 1960)

$$S_{\text{tot}} = S_{\text{in}} + S_{\text{nl}} + S_{\text{ds}}, \tag{1.2}$$

where S_{in} represents the atmospheric input from the wind, S_{nl} the nonlinear interactions between spectral components and S_{ds} dissipation due to white-capping and other processes. These source terms represent the physical processes involved, and their accurate representation is required to model correctly the evolution of the spectrum.

Early models (Pierson *et al.* 1966; Gelci & Devillaz 1970; Gelci & Chavy 1978) represented S_{tot} as the sum of processes representing atmospheric input and dissipation only. Later models (SWAMP 1985) recognized the importance of nonlinear interactions and included a variety of approximate representations for S_{nl}.

The organization of this paper is as follows. Section 2 provides the basic equations describing the nonlinear interactions in a gravity-wave spectrum. Solution techniques, ranging from full to parametric, are discussed in §3. Properties of the nonlinear interactions are investigated in §4. Here attention is paid to spectral evolution, shape stabilization and directional spread. Finally, conclusions are given in §5.

2. Formulation of the nonlinear source term, S_{nl}

To first order, ocean waves can be regarded as the superposition of free and independent spectral components. At higher order, however, there is an interaction between spectral components resulting in a transfer of energy (Phillips 1960). A general perturbation theory for the nonlinear resonant interaction of waves in a random sea was developed by Hasselmann (1962, 1963*a*, *b*). He found that a set of four waves, called a tetrad or quadruplet, could exchange energy when the following resonance conditions are satisfied:

$$\boldsymbol{k}_1 + \boldsymbol{k}_2 = \boldsymbol{k}_3 + \boldsymbol{k}_4, \tag{2.1}$$

$$\omega_1 + \omega_2 = \omega_3 + \omega_4, \tag{2.2}$$

in which ω_j is the radian frequency and $\boldsymbol{k}_j$ the wavenumber ($j = 1, \ldots, 4$). The frequency and the wavenumber are related by the dispersion relation $\omega^2 = gk \tanh(kh)$, where g is the gravitational acceleration and h the water depth. The four interacting wave components are described as a quadruplet.

Hasselmann (1963*a*) described the nonlinear interactions between wave quadruplets in terms of their action density, n, where $n(\boldsymbol{k}) = F(\boldsymbol{k})/\omega$. The rate of change in action density at $\boldsymbol{k}_1$ due to all quadruplet interactions involving $\boldsymbol{k}_1$ is

$$\frac{\partial n_1}{\partial t} = \iiint G(\boldsymbol{k}_1, \boldsymbol{k}_2, \boldsymbol{k}_3, \boldsymbol{k}_4) \times \delta(\boldsymbol{k}_1 + \boldsymbol{k}_2 - \boldsymbol{k}_3 - \boldsymbol{k}_4) \times \delta(\omega_1 + \omega_2 - \omega_3 - \omega_4)$$
$$\times [n_1 n_3 (n_4 - n_2) + n_2 n_4 (n_3 - n_1)] \, \mathrm{d}\boldsymbol{k}_1 \mathrm{d}\boldsymbol{k}_2 \mathrm{d}\boldsymbol{k}_3, \tag{2.3}$$

where $n_i = n(\boldsymbol{k}_i)$ is the action density at wavenumber $\boldsymbol{k}_i$ and G is a complicated coupling coefficient (Herterich & Hasselmann 1980; Van Vledder 1990). (The coupling coefficient originally given in Hasselmann (1962) is correct only for deep water, a finite depth term having been neglected.) The delta functions in (2.3) ensure that contributions to the integral only occur for quadruplets that satisfy the resonance conditions (2.1) and (2.2). The integral expression (2.3) is also known as the

PHILOSOPHICAL TRANSACTIONS OF THE ROYAL SOCIETY A MATHEMATICAL, PHYSICAL & ENGINEERING SCIENCES

Boltzmann integral for wind waves, in analogy to similar expressions used in theoretical physics to describe the rate of change of particle density distributions in a system of interacting particles.

The nonlinear energy transfer represented by (2.3) conserves both the total energy and momentum of the wave field, merely redistributing it within the spectrum. As a consequence of the symmetry of the resonance conditions with respect to the pairs of wavenumbers $(\boldsymbol{k}_1, \boldsymbol{k}_2)$ and $(\boldsymbol{k}_3, \boldsymbol{k}_4)$, the quadruplet interactions also conserve the wave action. The absolute value of the rate of change of the action density is equal for all wavenumbers within the quadruplet

$$\mathrm{d}n_1/\mathrm{d}t = \mathrm{d}n_2/\mathrm{d}t = -\mathrm{d}n_3/\mathrm{d}t = -\mathrm{d}n_4/\mathrm{d}t. \tag{2.4}$$

This result is known as the property of detailed balance (Hasselmann 1966). In a more general form, detailed balance states that the absolute value of the change in action density, $|\Delta n_j|$, is the same for all components in a resonant set of wavenumbers.

3. Solution techniques

Numerous techniques have been proposed for the solution of (2.3). The major goals of all these techniques have been two fold: to improve computational speed to the point where it becomes possible to include S_{nl} in routine wave prediction models and to provide a better physical understanding of the source term. Enormous progress has been made in these endeavours through the use of both approximations to the integral and improved numerical techniques.

The significant computational times required for the solution arise from two sources, first, (2.3) being a six-dimensional integral and, secondly, the complexity of the coupling coefficient G. Hasselmann (1963*b*), Sell & Hasselmann (1972), Webb (1978) and Masuda (1981) first removed the delta functions by projecting the six-dimensional integral onto the three-dimensional resonance subspace defined by (2.1) and (2.2). Although the details of the various projections differ, the goal was the same. This process introduces integrable singularities in the solution, which were removed either by the use of stretched coordinates or by indenting the solution around the singularities. The integral was then solved using direct integration techniques.

A major conceptual difficulty arises in attempting to visualize the interaction space due to the multi-dimensionality of the problem. Based on a suggestion by M. S. Longuet-Higgins, Hasselmann (1963*b*) proposed the following graphical representation of the interaction space. For deep-water conditions, where the dispersion relation reduces to $\omega^2 = gk$, (2.1) and (2.2) become

$$\boldsymbol{k}_1 + \boldsymbol{k}_2 = \boldsymbol{k}_3 + \boldsymbol{k}_4 = \boldsymbol{k}, \tag{3.1}$$

$$\sqrt{k_1} + \sqrt{k_2} = \sqrt{k_3} + \sqrt{k_4} = \gamma\sqrt{k}. \tag{3.2}$$

Normalizing, such that $k = 1$ and representing the angle between $\boldsymbol{k}_1$ and $\boldsymbol{k}$ as $\hat{\alpha}$ yields

$$\cos\hat{\alpha} = [1 + k_1^2 - (\gamma - \sqrt{k_1})^4]/2k_1. \tag{3.3}$$

For a fixed value of γ, the locus of all values of $\boldsymbol{k}_1$ which satisfy the resonance conditions is given by (3.3). The corresponding $\boldsymbol{k}_2$ is given by (3.1). Typical interaction curves for a given value of $\boldsymbol{k}$ but different values of γ are illustrated in figure 1.

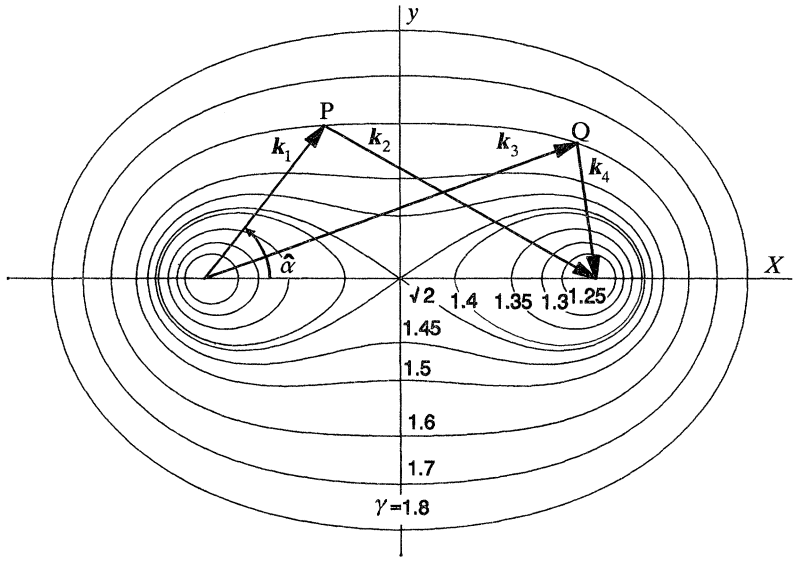

Figure 1. Interaction space diagram for a given value of $\boldsymbol{k} = \boldsymbol{k}_1 + \boldsymbol{k}_2 = \boldsymbol{k}_3 + \boldsymbol{k}_4$. Each curve is for a specific value of γ (after Phillips 1960; Hasselmann 1963*b*).

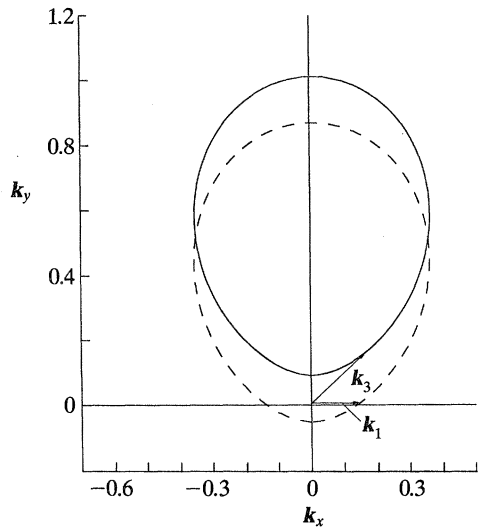

Figure 2. Loci of the vectors of $\boldsymbol{k}_2$ (——) and $\boldsymbol{k}_4$ (– – –) for a given combination of $\boldsymbol{k}_1$ and $\boldsymbol{k}_3$.

A similar and perhaps more straightforward representation of the interaction space was presented by Webb (1978). For $\boldsymbol{k}_1$ and $\boldsymbol{k}_3$ fixed, the locus of the possible values of $\boldsymbol{k}_2$ and $\boldsymbol{k}_4$ which will close the vector polygon represented by (2.1) and also satisfy (2.2), traces out two 'egg-shaped' figures. Figure 2 shows the loci of $\boldsymbol{k}_2$ and $\boldsymbol{k}_4$ for the case where $\boldsymbol{k}_1 = 0.14$ rad m^{-1} and $\boldsymbol{k}_3 = 0.20$ rad m^{-1}. The $\boldsymbol{k}_1$ vector is in the x direction and $\boldsymbol{k}_3$ is 45° clockwise from $\boldsymbol{k}_1$. For this combination of $\boldsymbol{k}_1$ and $\boldsymbol{k}_3$, only wavenumber components which lie on these loci will satisfy the resonance conditions and contribute to the integral.

The direct integration techniques mentioned above provided valuable insight into

the basic properties of the nonlinear source term, S_{nl}, but were computationally too expensive for use in wave prediction models. As a result, approximations for narrow-peak spectra have been proposed by Longuet-Higgins (1976), Fox (1976), Herterich & Hasselmann (1980) and Dungey & Hui (1980). Although these approximations capture many of the qualitative features of the interactions, such as the 'plus–minus' lobe structure, they do not reproduce other features, notably shape stabilization (see §4). Hence they are not flexible enough for use in a wave prediction model.

Hasselmann & Hasselmann (1981, 1985*b*) proposed a symmetric integration technique which significantly increased computational speed. Rather than considering the asymmetrical integral (2.3), which represents the change in energy of a fixed wavenumber $\boldsymbol{k}_1$ as a result of its interaction with all other combination of $\boldsymbol{k}_2$, $\boldsymbol{k}_3$ and $\boldsymbol{k}_4$, they used the property of detailed balance (2.4) to make the interaction symmetric. Applying this principle, the changes Δn_j in the action density per unit time of each of the components in the interaction are

$$\begin{Bmatrix} \Delta n_1 \\ \Delta n_2 \\ \Delta n_3 \\ \Delta n_4 \end{Bmatrix} = \begin{Bmatrix} +1 \\ +1 \\ -1 \\ -1 \end{Bmatrix} \cdot \mathrm{d}W, \tag{3.4}$$

where

$$\mathrm{d}W = \tilde{G} \cdot \tfrac{1}{4} P \cdot \boldsymbol{k}_1 \cdot \boldsymbol{k}_2 \cdot \boldsymbol{k}_3 \cdot \boldsymbol{k}_4,$$

$$\tilde{G} = G\delta(\boldsymbol{k}_1 + \boldsymbol{k}_2 - \boldsymbol{k}_3 - \boldsymbol{k}_4)\,\delta(\omega_1 + \omega_2 - \omega_3 - \omega_4),$$

$$P = n_1 n_3 (n_4 - n_2) + n_2 n_4 (n_3 - n_1).$$

By using this approach, the change in action density at each of the four wavenumbers is directly calculated for each interaction. This represents a four-fold reduction in computational effort compared with a direct solution of (2.3). In addition, Hasselmann & Hasselmann (1981) show that this symmetric form also enables effective use of all possible symmetries within the integral and coupling coefficient to further reduce computational effort. Further savings are made by filtering the interaction space for use in subsequent computations. Hasselmann & Hasselmann (1981) showed that only 5–10% of the interacting wavenumber quadruplets contribute 95% of the nonlinear transfer. The result is a decrease in computational time by a factor of up to 100 (Hasselmann & Hasselmann 1981). One disadvantage of this approach is that the nature of the solution technique leads to computer code that is not easily vectorizable (Van Vledder & Weber 1988) and hence full use cannot be made of modern super computers. In a wave model, however, computational efficiency can still be gained by structuring an inner vector loop over the computational grid points or over a number of different cases to be run (Komen *et al.* 1984).

Despite the fact that it could not be vectorized, this symmetric integration technique was still computationally efficient enough to enable the development of the one-dimensional wave mode EXACT-NL (Hasselmann & Hasselmann 1985*a*). This model solved the energy balance equation (1.1) for the one-dimensional cases of either fetch or duration limited growth. A full two-dimensional solution of (1.1) was still not feasible despite the computational efficiency of the symmetric integration technique. EXACT-NL has proven a useful vehicle for the investigation of a number of processes. Komen *et al.* (1984) have investigated the fully developed wind–sea

spectrum, Young *et al.* (1987) and Van Vledder & Holthuijsen (1992) the response of the spectrum to turning winds, and Weber (1988) the energy balance in water of finite depth.

Hasselmann & Hasselmann (1981) indicate that for deep water, the interaction space diagram in figure 1 need not be redrawn for different values of $\boldsymbol{k}$. These diagrams simply being related by a scale factor. Hence, it is necessary only to calculate one interaction space diagram and its associated set of coupling coefficients, all others being defined by the scaling laws. This feature was used in Hasselmann's (1963*a*) original computations. However, to maintain program generality for finite depth waves this additional property was not used in EXACT-NL.

The solution technique proposed by Webb (1978) involved reducing the multi-dimensional integral represented by (2.3) to a series of line integrals around the 'egg-shaped' loci resulting from the projection used to remove the delta functions. Although this operation simplifies the mathematical formulation of the problem, the number of possible loci along which line integrals need be performed is enormous. Hence, the technique is still computationally expensive.

Tracy & Resio (1982) and Resio & Perrie (1991) showed, in a similar manner to Hasselmann & Hasselmann (1981), that for deep-water conditions, these loci were geometrically similar. In addition, the line integrals for different loci could be related using a simple scaling relation. To take maximum advantage of the form of the deep water dispersion relation and the similarity scaling for the loci, a computational wavenumber grid of the form $k_i = ak_{i-1}$, where a is a constant was adopted.

Although their solution technique does not take advantage of all the symmetries used by Hasselmann & Hasselmann (1981), the more direct solution technique is easily vectorized. The end result is that the computation times required for both solutions are comparable.

To incorporate the effects of nonlinear interactions into two-dimensional wave prediction models, various techniques have been proposed to parametrize S_{nl} in relatively simple and computationally efficient forms (Barnett 1968; Ewing 1971; Hasselmann *et al.* 1985; Young 1988). Models which have used these parametrizations are referred to as second generation as opposed to first generation models that neglected S_{nl} completely, artificially enhancing S_{in} to obtain satisfactory growth rates. Although model performance was improved by the addition of these parametric forms, the simple representations of S_{nl} had significantly less degrees of freedom than the discrete spectral grid and hence were not flexible enough to be completely successful. These parametrizations of S_{nl} lose most of the essential physics of the Boltzmann integral (see §4).

This problem was overcome by Hasselmann *et al.* (1985) in their discrete interaction approximation (DIA) to the Boltzmann integral. Whereas a full solution of (2.3) uses a very large set of wavenumber quadruplets with many different configurations, the DIA uses a rather small number of quadruplets which all have the same configuration. The chosen configuration has $\boldsymbol{k}_1 = \boldsymbol{k}_2$, where $\boldsymbol{k}_3$ and $\boldsymbol{k}_4$ are of different magnitude and lie at an angle to the first two wavenumbers. The corresponding four frequencies are related by

$$\left.\begin{aligned} f_1 &= f_2 = f, \\ f_3 &= f(1+\lambda) = f^{+}, \\ f_4 &= f(1-\lambda) = f^{-}, \end{aligned}\right\} \tag{3.5}$$

where $\omega = 2\pi f$.

The four wavenumbers must also satisfy the resonance condition (2.1), (3.5) ensuring that (2.2) is satisfied. Empirically, Hasselmann *et al.* (1985) set $\lambda = 0.25$. The rates of change of the energy densities $(\delta S_{\mathrm{nl}}, \delta S^{+}_{\mathrm{nl}}, \delta S^{-}_{\mathrm{nl}})$ within one such wavenumber quadruplet are given by

$$\begin{Bmatrix} \delta S_{\mathrm{nl}} \\ \delta S^{+}_{\mathrm{nl}} \\ \delta S^{-}_{\mathrm{nl}} \end{Bmatrix} = \begin{Bmatrix} 2 \\ -1 \\ -1 \end{Bmatrix} C g^{-4} f^{11} \left[E^2 \left(\frac{E^+}{(1+\lambda)^4} + \frac{E^-}{(1-\lambda)^4} \right) - 2 \frac{E E^+ E^-}{(1-\lambda^2)^4} \right], \tag{3.6}$$

where g is gravitational acceleration, C is a constant equal to 3×10^7 and E, E^+ and E^- are the energy densities (expressed in polar, frequency-direction space, $E(f, \theta) = kdk/dfF(\boldsymbol{k})$) at the interacting wavenumbers. The wavenumber associated with E occurs at a spectral grid point whereas those associated with E^+ and E^- are generally at non-grid points. These energy densities must be determined by interpolation from the discrete spectrum. Hence, the parametrization represented by (3.6) has the same number of degrees of freedom as the spectrum. The interaction combination represented by (3.5) is only one of many which could have been used. No major systematic attempts have been made to optimize the choice.

To compute the nonlinear transfer for a given energy spectrum, all interactions between four wavenumbers satisfying the resonance conditions (2.1) and (3.5) are considered, and for which the central wavenumber $\boldsymbol{k}$ $(= \boldsymbol{k}_1 = \boldsymbol{k}_2)$ loops over all wavenumbers of the discretized spectrum. This reduces the problem to a two-dimensional integral rather than a six-dimensional integral required for a full solution. Typically, the number of interactions is reduced by three orders of magnitude.

Despite the fact that the number of interacting wavenumbers considered in the DIA is only a small fraction of those used in the full solution, the approximation retains the essential physical properties of the Boltzmann integral. Hence, the DIA reasonably accurately reproduces the basic properties of the nonlinear interactions. These properties of the full Boltzmann integral are discussed in §4. Naturally, the neglect of so many possible interactions has consequences. One example of this is that the DIA typically produces spectra with broader directional spreading than do models with a full solution to S_{nl} (Young *et al.* 1987; Van Vledder 1990). The DIA has, however, resulted in the development of the first third generation global wave model, WAM (WAMDI 1988). An extension of this model to include shallow water effects and wave-current interactions has been presented by Tolman (1991) and also in Cycle 4 of the WAM model (Günther *et al.* 1991).

4. Properties of the nonlinear transfer

(*a*) *Spectral evolution*

Because of the complexity of the Boltzmann integral (2.3) an understanding of the nature of the integral and the role it plays in the evolution of wind-waves is best obtained through numerical experiment. This was achieved to some extent during JONSWAP (Hasselmann *et al.* 1973), where S_{nl} was evaluated for idealized fetch limited spectra at various fetches ranging from very 'young' seas to almost fully developed states. One problem with this approach is that the nonlinear transfer is very sensitive to the spectral shape. Hence, imposing a spectral shape which is, at best, an approximation to observed spectra may yield misleading results. Small differences in the spectral shape can result in quite large differences in the computed

PHILOSOPHICAL TRANSACTIONS OF THE ROYAL SOCIETY A MATHEMATICAL, PHYSICAL & ENGINEERING SCIENCES

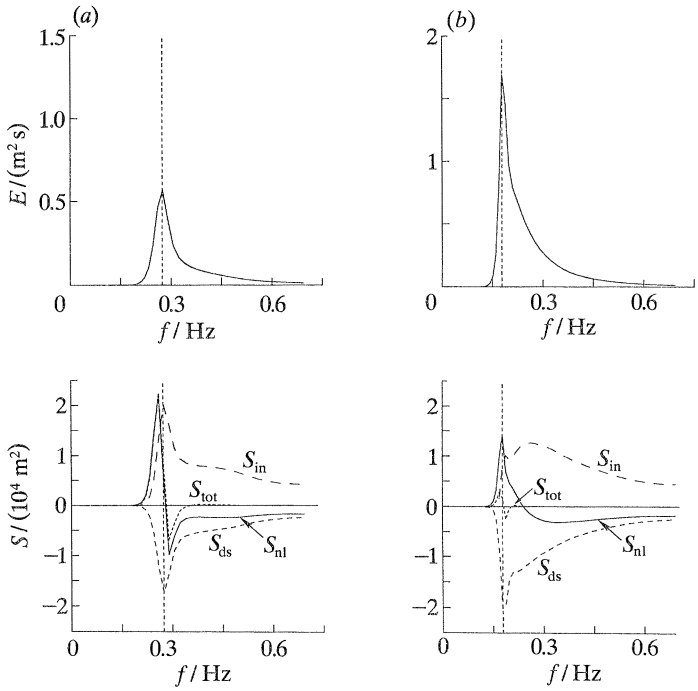

Figure 3*a*. The one-dimensional spectrum (above) and the source terms for a spectrum at short fetch. The wind speed is $U_{10} = 10$ m s^{-1}. The position of the spectral peak is shown with a vertical dashed line.

Figure 3*b*. The one-dimensional spectrum (above) and the source terms for a spectrum approaching a fully arisen condition (asymptotic state). The wind speed is $U_{10} = 10$ m s^{-1}. The position of the spectral peak is shown with a vertical dashed line.

S_{nl}. This was shown by Komen *et al.* (1984) where they attempted to determine the dissipation term required to balance the other source terms for an assumed 'fully developed' Pierson–Moskowitz (Pierson & Moskowitz 1964) spectrum. As the Pierson–Moskowitz spectrum is only an approximation to the fully developed form and as some directional spread must be assumed, no plausible balancing dissipation could be found. Instead, they inverted the problem by using the one-dimensional EXACT-NL model (Hasselmann & Hasselmann 1985*a*). They allowed the two-dimension spectrum to develop under the action of the source terms and determined the dissipation term required to produce an asymptotic state close to the Pierson–Moskowitz form.

A similar one-dimensional model has been used here. For the case of deep water and steady state fetch limited growth (1.1) reduces to

$$C_{\mathrm{g}} \cos\theta \frac{\partial E}{\partial x} = S_{\mathrm{tot}}, \tag{4.1}$$

where $E = E(f, \theta)$, is the directional frequency spectrum, θ is the angle between the x direction and the spectral component and x is the fetch. The source terms used to define S_{tot} are identical to those of Komen *et al.* (1984) except that the computational technique of Tracy & Resio (1982) and Resio & Perrie (1991) was used for S_{nl}.

The directional frequency spectrum $E(f, \theta)$ was defined on a polar grid. A total of

37 angular bands were defined in the range $\pm 120°$ of the wind direction, thus yielding a directional resolution of 6.67°. A logarithmic wavenumber spacing consisting of 43 bands spaced according to the relation $k_i = 1.13k_{i-1}$, with $k_0 = 2 \times 10^{-2}$ rad m^{-1}. Hence, the highest spectral component resolved by the model was 3.39 rad m^{-1} (0.92 Hz). Resio & Perrie (1991) have investigated a number of spectral resolutions and found choices comparable with the one utilized here to be adequate.

The solution technique of Tracy & Resio (1982) and Resio & Perrie (1991) for S_{nl} was adopted over the better known technique of Hasselmann & Hasselmann (1981) as it is slightly more computationally efficient. A number of comparisons with the published results of Hasselmann & Hasselmann (1981) were performed to ensure the two methods produced comparable results. The results are almost identical, minor differences occur however due to the different computational grid formulations used by the two techniques.

In keeping with the suggestions of Resio & Perrie (1991), the loci, around which the line integrals were performed were discretized with 50 points. Although the values of spectral energy are defined at each of the $\boldsymbol{k}_1, \boldsymbol{k}_3$ points, the $\boldsymbol{k}_2, \boldsymbol{k}_4$ values, which make up the loci, will generally be at non-grid points and the energy at these points was evaluated using bi-linear interpolation within the computational grid defining the $\boldsymbol{k}_1, \boldsymbol{k}_3$ points. It is also possible for the loci defining the $\boldsymbol{k}_2, \boldsymbol{k}_4$ points to extend beyond the high wavenumber cut-off of the computational grid. To include such interactions, the energy at such points was evaluated by extending the computational grid with a diagnostic tail (Hasselmann & Hasselmann 1981). Sensitivity tests were performed with a number of forms for this tail. Provided the explicit computational grid was extended to relatively high wavenumbers, as adopted above, the diagnostic tail extension only biased the last two or three computational points in the explicit grid. A form for this tail with $E(f) \propto f^{-4}$ was finally adopted. The constant of proportionality was set independently for each directional band so that the first energy bin of the diagnostic extension tail was equal to the last point in the explicit computational grid for that direction. Similarly, since the directional bands within the model are defined only in the region $\theta = \pm 120°$, some assumption must be made about the energy outside this range. Again a number of alternatives were investigated. Since there is little energy for directions greater than 120° to the wind, the final choice has little effect on the spectral evolution. For simplicity, it was assumed the $E(f, \theta)_{|\theta| > 120°} = E(f, \theta = 120°)$.

The initial condition selected for all runs consisted of a mean JONSWAP spectrum (spectral parameters: $\gamma = 3.3$, $\alpha = 0.01$, $\sigma_a = 0.07$ and $\sigma_b = 0.09$) with a $\cos^2 \theta$ directional spread. The peak frequency, f_p, was set at 0.3 Hz. Again, a number of sensitivity runs were performed with alternative initial spectral forms. As reported by Komen *et al.* (1984), model results are very insensitive to the assumed initial spectral form, the spectrum very quickly being shaped to a form consistent with the source terms. The only influence of the initial conditions is that it sets the initial total energy for the run.

Figure 3 shows the one-dimensional spectrum and the various source terms at two different fetches. A relatively 'young' sea at a short fetch is shown in figure 3*a*, whereas a mature spectrum approaching fully developed conditions appears in figure 3*b*.

The spectrum in figure 3*a* is typical of wind-seas at short fetches. There is a characteristic rapid rise to the spectral peak followed by a more gradual decline at higher frequencies. Both observations (Donelan *et al.* 1985; Banner 1990) and

theoretical arguments (Zakharov & Filonenko 1967) indicate this high frequency fall-off is approximately described by an f^{-4} form. The nonlinear source term S_{nl} shows a marked plus–minus signature with a narrow positive lobe at frequencies less than the spectral peak and a broad negative lobe at frequencies greater than the spectral peak. The distribution becomes positive again at frequencies higher than those shown in the figure. Previous presentations of S_{nl} have generally been for prescribed JONSWAP spectral forms, with the high frequency region proportional to f^{-5}. For such spectral shapes the negative lobe is relatively narrow. The S_{nl} terms for the f^{-4} spectra which naturally evolve from the model have a broad and almost constant magnitude negative lobe. The calculations of Resio & Perrie (1991) for f^{-4} spectra show the same structure. This clearly demonstrates the sensitivity of S_{nl} to spectral shape.

The atmospheric input S_{in} and the dissipation S_{ds} both peak at frequencies corresponding to the spectral peak frequency and slowly decay in magnitude with frequency. It is the sum of the source terms as represented by S_{tot} which determines the evolution of the spectrum. At high frequencies, all source terms balance such that $S_{tot} \approx 0$. As $S_{tot} \approx 0$, the magnitude of the spectral ordinates at these frequencies remains largely constant as a function of fetch, thus accounting for the commonly observed 'saturation' region, which is largely invariant as a function of fetch. With the source terms used in the present model, this region is characterized by a spectrum of a form approximately represented by f^{-4}. It should be noted, however, that the exact details of this region can be altered depending on the form adopted for S_{in} and S_{ds}. The nonlinear source term, S_{nl}, acts to always balance the sum of these terms. A number of different forms for S_{in} and S_{ds} have been investigated. The amount of energy in the spectral tail is quite sensitive to the actual choice. The spectral decay exponent, however, is less sensitive. With plausible formulations for S_{in} and S_{ds}, a spectrum of a form approximately equal to f^{-4} is a robust feature of the model.

At frequencies slightly above the spectral peak there is a marked negative lobe followed by a small positive lobe. This accounts for the undershoot/overshoot phenomenon reported by Barnett & Sutherland (1968). The large positive lobe at frequencies less than the spectral peak accounts for the increase of energy in the spectrum and the gradual migration of the spectral peak to lower frequencies with fetch.

As the spectrum grows, the peak frequency moves to lower frequencies and the spectrum broadens. Eventually it approaches an asymptotic state where growth almost stops (figure 3*b*). The peak in the atmospheric input term is now less well defined and occurs at a frequency higher than the spectral peak. This occurs since the energy transfer to waves with a phase speed approaching the wind speed is small. The dissipation remains similar to the case in figure 3*a* with a marked peak at the spectral peak frequency. The nonlinear term, however, changes shape dramatically, with its magnitude now much reduced. This is a result of the frequency dependence of the coupling coefficient, G, as well as the broader spectral shape. The broadening in the spectral shape changes the relative energy in each of the components in the number density product term $[n_1 n_3(n_4 - n_2) + n_2 n_4(n_3 - n_1)]$ in (2.3) and hence the overall form of S_{nl}. The positive lobe now moves to a frequency equal to the spectral peak frequency and almost balances the other source terms. The net result is that a source term balance is achieved across all frequencies and growth almost completely halts.

Although all the source terms contribute to the source term balance, it is S_{nl} that plays the critical role. Current representations for both S_{in} and S_{ds} have few degrees

PHILOSOPHICAL TRANSACTIONS OF THE ROYAL SOCIETY A MATHEMATICAL, PHYSICAL & ENGINEERING SCIENCES

of freedom and hence can only change shape marginally with spectral evolution. Because of its inherent flexibility, however, S_{nl} can change its shape dramatically as the spectrum develops. Thus a very different source term balance at different stages of spectral development is achieved.

An obvious aid to the understanding of the nature of S_{nl} would be an appreciation of which interacting quadruplets provide a significant contribution to the integral (2.3). A complete understanding is not possible due to the huge number of interactions. Some insight can, however, be gained by investigating the magnitude of the various terms in the integral for specific interaction combinations (Hasselmann 1963*b*). For wavenumber quadruplets which satisfy the resonance conditions, (2.3) can be considered as the product of two terms, the coupling coefficient G and the number density product term $[n_1 n_3(n_4-n_2)+n_2 n_4(n_3-n_1)]$. To determine the relative contribution of these two terms, a prescribed spectral shape must be adopted. For the present application a mean JONSWAP spectrum with a peak frequency of $f_p = 0.3$ Hz and a $\cos^2\theta$ directional distribution has been selected.

Figure 4 shows the loci of values of $\boldsymbol{k}_2$ and $\boldsymbol{k}_4$ for selected values of $\boldsymbol{k}_1$ and $\boldsymbol{k}_3$ (following Webb 1978). The loci are divided using reference marks numbered 1 to 10. Each diagram is for a specific pair of wavenumbers $\boldsymbol{k}_1$ and $\boldsymbol{k}_3$. For such a combination, a vector drawn to, for example, reference point 8 on the $\boldsymbol{k}_2$ locus would be one possible value of $\boldsymbol{k}_2$ in a quadruplet. The corresponding value of $\boldsymbol{k}_4$ would be represented by a vector drawn to reference point 8 on the $\boldsymbol{k}_4$ locus. In addition, the value of the coupling coefficient, number density product term and the total product of these two terms is shown as a function of distance, s (in wavenumber space), measured along the loci. The reference marks used on the loci are also reproduced on these figures. Thus, the values of each of the terms at, for example, reference point 8 would correspond to the quadruplet mentioned above. In its present form, figure 4 shows the transfer of energy to or from the wavenumber component $\boldsymbol{k}_1$. By using the property of detailed balance (equation (2.4)) it is possible to determine the transfers at each of the other wavenumber components in the interaction. Figure 4*a* shows the case for $\boldsymbol{k}_1 = 0.3622$ rad m^{-1}, corresponding to the spectral peak wave number and $\boldsymbol{k}_3 = 0.4$ rad m^{-1}. Both wavenumbers are in the mean direction of the spectrum. As could have been expected, the loci are symmetrically distributed about the mean wave direction. The coupling coefficient peaks for the case of all wavenumbers in the same direction (reference point 6). This case, however, corresponds to $\boldsymbol{k}_1 = \boldsymbol{k}_4$ and $\boldsymbol{k}_2 = \boldsymbol{k}_3$ for which the number density product term becomes zero. The total product term and hence the contribution to the integral peaks for $\boldsymbol{k}_2$ and $\boldsymbol{k}_4$ directed slightly away for the mean spectral direction. Because of the cubic nature of the number density product term (i.e. products of the form $n_1 n_3(n_4-n_2)$, etc.) and the typical narrow peak shape of the spectrum, the resulting contribution to the integral is very peaked as a function of wavenumber measured around the locus. The coupling coefficient favours quadruplets that are aligned, but when multiplied by the number density product term, which is close to zero for such interactions, they contribute little to the final integral. Thus, the importance of a directional distribution is demonstrated. Indeed, since the nonlinear interaction transfers energy between the spectral peak and other directions (as demonstrated by figure 4*a*), they ensure a directional sea develops. The directional distribution is hence not simply a result of the component of the wind in a given direction. It is coupled through the nonlinear terms to the whole spectrum. This accounts for the similarity of measured directional spreads in wind–sea spectra. They are a property

PHILOSOPHICAL TRANSACTIONS OF THE ROYAL SOCIETY A MATHEMATICAL, PHYSICAL & ENGINEERING SCIENCES

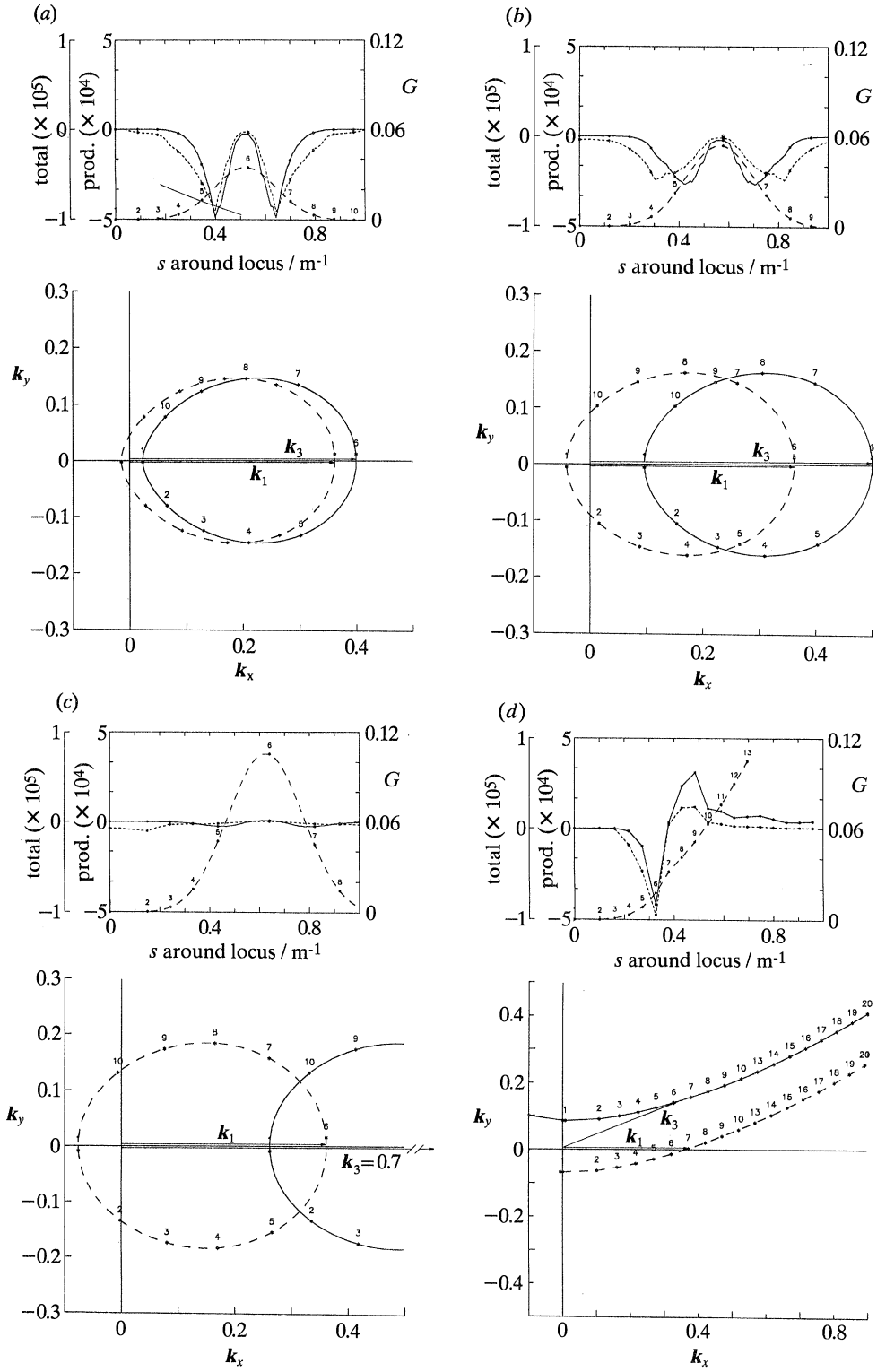

Figure 4*a–d*. For description see opposite.

PHILOSOPHICAL TRANSACTIONS OF THE ROYAL SOCIETY A MATHEMATICAL, PHYSICAL & ENGINEERING SCIENCES

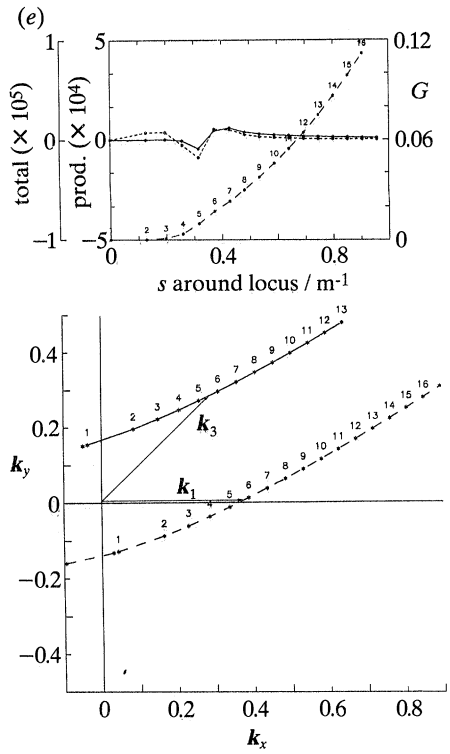

Figure 4*a–e*. Loci of $\boldsymbol{k}_2$ (——) and $\boldsymbol{k}_4$ (– – –) for the given combination of $\boldsymbol{k}_1$ and $\boldsymbol{k}_3$ together with (top panel) values of the coupling coefficient, G (—— ——), the product term (– – – –), and the product of these two terms (——) for various points around the loci. The reference marks (1–10) around the loci correspond to the numbers on the curves of the three calculated quantities.

of the spectrum partly determined by the nonlinear term as are features such as the f^{-4} high-frequency decay. Naturally, S_{nl} is not the only term responsible for the directional distribution, both S_{in} and S_{ds} also play a role. In addition, other processes such as wind gustiness (both in speed and direction) as well as varying fetch length which exists in cases such as slanting fetches also have an influence. It is interesting to note that if the spectrum consisted purely of components propagating in the same direction, the number density product term and hence S_{nl} would always be zero. If, however, there is even a small amount of energy at angles to the mean direction it will provide the initial seed required for S_{nl} to shape a directional distribution.

The plot of the number density product term in figure 4*a* appears to be rather jagged. This is a direct result of the numerical technique used for its evaluation. To evaluate this term it is necessary to know n_1, n_2, n_3 and n_4. In the formulation used here the computational grid defines $\boldsymbol{k}_1$ and $\boldsymbol{k}_3$ and hence n_1 and n_3. As $\boldsymbol{k}_2$ and $\boldsymbol{k}_4$ are generally at non-grid points, n_2 and n_4 must be evaluated by interpolation within the k_1, k_3 grid. Tests have shown that, because of the cubic nature of the product term it is very sensitive to the accuracy of this interpolation. The result is the jagged appearance of the plot. An ongoing debate among researchers in this field is why many of the calculations of S_{nl} obtained with EXACT-NL also appear rather ragged. This ragged or fine scale structure can be explained in a similar fashion (K. Hasselmann, personal communication). In a similar manner to the S_{nl} implemen-

tation used in the present model, EXACT-NL represents the interaction space and the spectrum on separate grids. The change in energy associated with a quadruplet interaction, as calculated on the interaction grid, is assigned to the appropriate wavenumber component on the spectral grid using an interpolation scheme. Generally, the resolution of the spectral grid is coarser than the interaction grid. If, however, it is finer, each spectral bin will only have a small number of interactions associated with it and the resulting transfer will be ragged. In this case, the output nonlinear transfer rate should be smoothed to a resolution compatible with the interaction space resolution used in the integration.

Figure 4*b*, *c* shows the cases for the same value of $\boldsymbol{k}_1$ as above but with $\boldsymbol{k}_3$ gradually increasing. Again both wavenumbers are aligned in the mean wave direction. The loci become larger as the difference between the two wavenumbers increases. Despite the fact that the coupling coefficient increases slightly in magnitude, the larger loci ensure more interacting wavenumbers are in regions of the spectrum where there is little energy. Hence the product term reduces rapidly as $\boldsymbol{k}_1$ and $\boldsymbol{k}_3$ are moved further apart, resulting in a rapid decrease in the contribution to the integral. The transfer is consequently largely determined by the typically peaked spectral shape. This explains why the narrow peak approximations to the integral are successful in reproducing the qualitative features of the energy transfer. The dominance of the spectral peak in determining the magnitude of S_{nl} also explains the success of parametric representations for the wind–sea spectrum expressed in terms of spectral peak parameters. The comprehensive study of Donelan *et al.* (1985), for instance, shows that f_{p}, the spectral peak frequency and C_{p}, the phase speed at the spectral peak are important parameters in determining not only the one-dimensional spectral shape but also the directional spread.

Figure 4*d*, *e* shows the result of separating $\boldsymbol{k}_1$ and $\boldsymbol{k}_3$ in direction. The values of these wavenumbers are the same as figure 4*a* but they are directed such that $\boldsymbol{k}_1$ is in the mean wave direction and $\boldsymbol{k}_3$ is at 22.5° in figure 4*d* and 45° in figure 4*e*. As the directional separation increases, the size of the locus increases rapidly and the magnitude of both the coupling coefficient and number density product terms decrease. The symmetry of the transfer is now lost and the characteristic 'plus–minus' shape of the transfer becomes apparent. Again the narrow peak shape of the spectrum dominates the transfer.

The interactions shown in figure 4 represent only a small fraction of those possible but they demonstrate that for typical spectral shapes, the significant interactions are for wavenumbers concentrated near the spectral peak in both wavenumber and direction. Hence, the position of the spectral peak and its magnitude play a dominant role in defining S_{nl} and hence in controlling the spectral shape.

(*b*) *Shape stabilization*

Although the role of S_{nl} in determining the evolution of the spectrum is of great significance, it also has an important role in stabilizing the shape of the spectrum. This is best illustrated by applying a perturbation to the spectrum and then investigating the source term response. The one-dimensional model described by (4.1) was allowed to evolve for a period from a prescribed initial condition under the action of the wind. A perturbation was then induced by reducing the magnitude of all spectral components of the directional spectrum at a given frequency by a value of 50%. The model run was then continued to investigate the response to the perturbation. Figure 5 shows the response of the spectrum and the source terms to

PHILOSOPHICAL TRANSACTIONS OF THE ROYAL SOCIETY A MATHEMATICAL, PHYSICAL & ENGINEERING SCIENCES

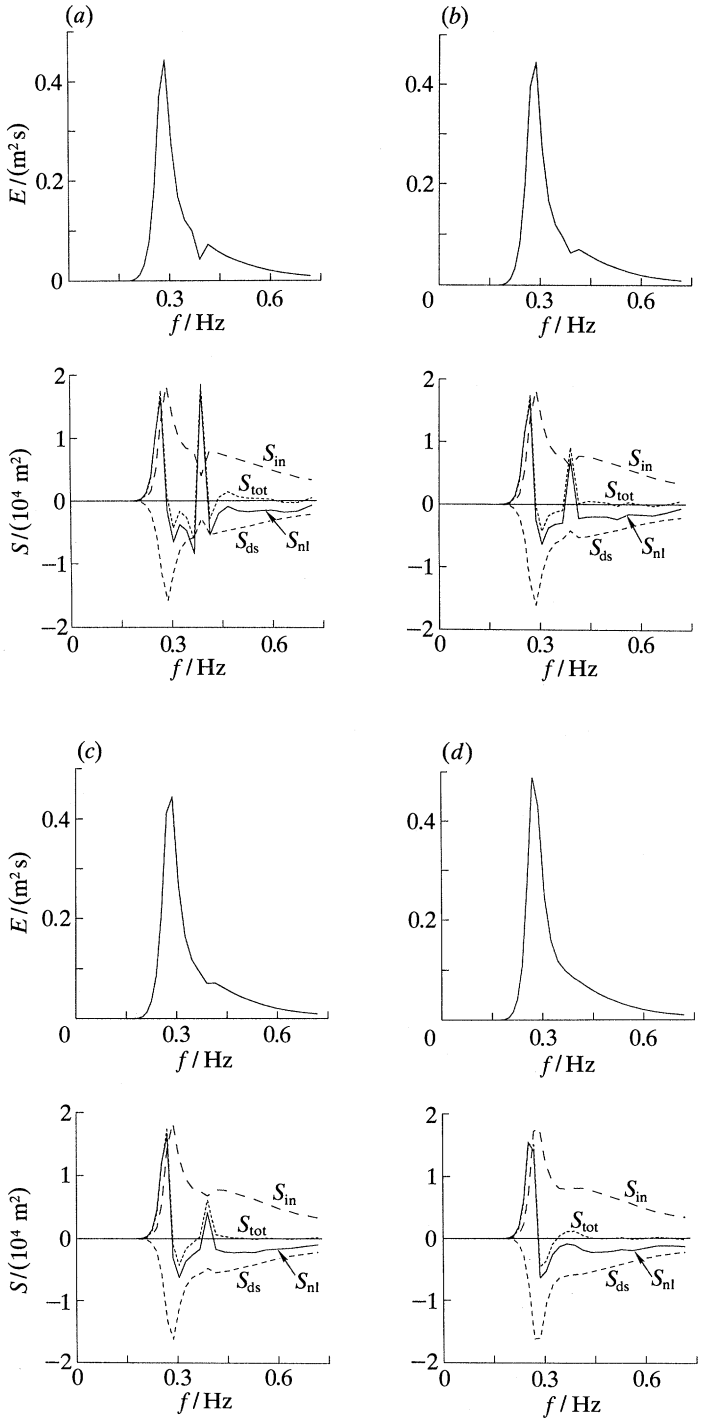

Figure 5. The evolution of a spectrum following a perturbation of the spectral level. The spectrum together with the source term balance are shown at four times following the perturbation. The figures are at times of (*a*) 0, (*b*) 180, (*c*) 300 and (*d*) 900 s after the introduction of the perturbation, respectively.

PHILOSOPHICAL TRANSACTIONS OF THE ROYAL SOCIETY A MATHEMATICAL, PHYSICAL & ENGINEERING SCIENCES

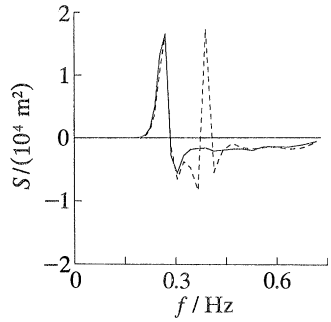

Figure 6. The nonlinear source term S_{nl} directly before (——) and directly after (– – – –) the perturbation of the spectrum. Energy flows from frequencies both above and below the perturbation frequency to smooth the perturbation.

the perturbation. The major response to the perturbation is caused by S_{nl}. A large positive input is directed to the frequency where the spectral energy was reduced. This acts to fill the 'hole' created in the spectrum. As can be seen by the series of diagrams in figure 5*a–d* the result is that the perturbation is gradually smoothed out. As total energy must be conserved by the nonlinear terms, the positive energy fed into the perturbed region must be balanced by a decrease in the transfer in other regions. Figure 6 provides a comparison of S_{nl} immediately before and after the introduction of the perturbation. The energy transferred to the region where the perturbation has occurred comes from components of the spectrum immediately neighbouring the perturbed region. Hence, the stabilization can be viewed as a flow of energy from neighbouring wavenumbers to the perturbed region.

This type of behaviour by the nonlinear terms ensures that the spectrum always remains stable. Any perturbations which develop are smoothed to ensure the spectrum always reverts to a unimodal form with an approximately f^{-4} high frequency decay. It is probable that such processes are always occurring in nature. Any slight imbalances in the spectrum caused by locally enhanced dissipation or gustiness in the wind are compensated by the nonlinear interactions.

This feature has advantageous side effects in the field of numerical modelling. Models such as the one being used here become insensitive to the initial conditions. The nonlinear terms simply shape the initially chosen spectrum to the desired form irrespective of its initial shape. This also explains why models that either neglect S_{nl} completely (first generation models) or represent it in a parametric form with only a few degrees of freedom (second generation models) can only maintain stability in the high frequency region of the spectrum by applying a frequency dependent limit to growth. Since they either ignore S_{nl} or represented it very simply, the shape stabilizing effects can not be included.

As already reported by Young *et al.* (1987) and Van Vledder & Holthuijsen (1992) this effect also governs the response of the spectrum after a sudden wind shift. In such a case a new wind–sea peak could be expected to develop in the new wind direction. This would result in a bi-modal spectral shape which the nonlinear terms would act to erode. The end result is that the spectrum smoothly rotates to align with the new wind direction. If, however, the wind shift is very large, the nonlinear coupling between the new and old seas will be small, as illustrated in figure 4. A new wind–sea develops in the new wind direction, whereas the old spectrum becomes swell.

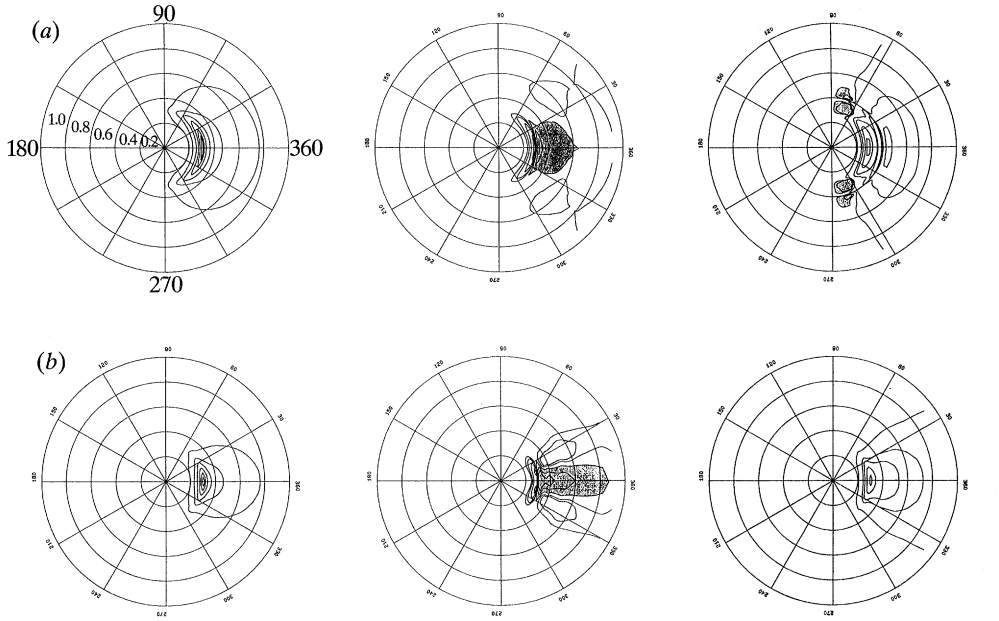

Figure 7. Isoline plots of the spectrum (left), S_{nl} (middle) and S_{tot} (right) for a directional spread of the form (*a*) $\cos^2\theta$ and (*b*) $\cos^{10}\theta$. Spectral contours are drawn at 0.01, 0.1, 0.25, 0.5, 0.75 and 0.9 times the spectral maximum. Contours of S_{nl} are drawn at -0.9, -0.5, -0.2, -0.1, 0.1, 0.2, 0.5 and 0.9 times the maximum positive value of S_{nl} and contours of S_{tot} at -0.05, -0.01, 0.1, 0.2, 0.5 and 0.9 times the maximum positive value of S_{tot}. Negative regions of S_{nl} and S_{tot} are shaded.

A similar feature has also been observed by the authors in the global WAM model. For artificial test cases where a uniform westerly wind is applied in the Southern Ocean, waves initially generated by the westerly wind could be expected to be gradually deflected towards the north as they propagate along their respective great circle paths. This, however, results in a skewed directional distribution to the spectrum. As the nonlinear terms favour a symmetric distribution, they force these components back to the south. Once the wind stops or decreases in magnitude, the spectral components disperse due to their differing group velocities, become swell like (single frequency or monochromatic) and hence the product term in (2.3) ensures the nonlinear terms are no longer important. The spectral components are then free to propagate along their great circle paths as swell. For practical cases, however, where spatial and temporal variability of the wind field exists, such effects are likely to be masked.

(*c*) *Directional spread*

The nonlinear terms also play a dominant role in determining the directional spread of the spectrum. Figure 7 shows polar isoline plots of the spectrum, S_{nl} and S_{tot} for two mean JONSWAP spectra with directional spreads of the form $\cos^2\theta$ (figure 7*a*) and $\cos^{10}\theta$ (figure 7*b*) respectively. Negative regions of S_{nl} and S_{tot} are highlighted by shading. The directionally narrow positive nonlinear transfer at frequencies less than the spectral peak is apparent in both cases. At frequencies above the spectral peak, the dominant nonlinear transfer is the negative lobe centred about the mean direction. As the angle to the mean direction increases, small positive lobes develop. These tend to broaden the directional spread at frequencies above the

spectral peak. The magnitude of these positive side lobes is greater for the narrower directional spread. Hence, at frequencies above the spectral peak, the nonlinear terms are acting to gradually broaden narrow spectra to a shape favoured by S_{nl}. The nonlinear terms do not act in isolation; atmospheric input and dissipation are also active. The action of all three is shown in S_{tot}. At frequencies above the spectral peak, S_{tot} is positive indicating both spectral shapes are continuing to grow and broaden. Near the spectral peak frequency, negative side lobes develop for the $\cos^2\theta$ distribution, thus tending to narrow the spectrum in this region. In this case the narrowing is not caused directly by S_{nl} but by S_{ds}. It is, however, indirectly controlled by S_{nl}. Once a stable directional spread is reached S_{nl} will act to balance the sum of S_{ds} and S_{in}. In effect, the nonlinear terms allow the dissipation to shape the spectrum in this case. The atmospheric input and dissipation are quasi-local in frequency space, depending only on integral properties of the spectrum and the local frequency. Hence, they cannot actively control the spectral shape. The nonlinear terms however couple all frequencies and control the spectral shape either directly, as in the case of the positive side lobes at high frequencies, or indirectly, as for the negative side lobes at low frequencies. They continually force the spectrum to a shape with a broader directional spread at high frequencies and a relatively narrow spread around the peak. This is consistent with observed directional data (Mitsuyasu *et al.* 1975; Hasselmann *et al.* 1980; Holthuijsen 1983; Donelan *et al.* 1985).

The exact form of the directional spreading will depend on the functional form of both S_{in} and S_{ds}, for which there is still uncertainty. Although alternate forms for these source terms will have a quantitative influence on the spreading, the general processes described above remain valid.

5. Conclusions

The complex role played by nonlinear interactions in determining the evolution of wind-waves has been reviewed. As a result of significant advances in the numerical techniques used to solve the Boltzmann integral, it is now possible to perform numerical experiments to more fully appreciate the many properties of these interactions. Although atmospheric input and dissipation can alter the growth rate of the spectrum, they alone are not flexible enough to account for the many observed features of wind-wave evolution. Nonlinear interactions account for the gradual migration of the spectral peak to lower frequencies with an increase in fetch. In addition, the commonly observed f^{-4} high frequency decay of the spectrum is a direct result of nonlinear interactions. Indeed, these interactions continually force the spectrum back to this shape when the spectrum is artificially perturbed from it. As a result, a self stabilizing effect is always present within the spectrum, thus accounting for the self-similar nature of wind-waves. The directional distribution of the wave spectrum and its functional dependence on frequency is also a result of nonlinear interactions. Although all the source terms are of similar magnitude, it is the nonlinear terms which play the critical central role in the development of the spectrum.

Hence it is clear that for routine wave prediction models it is necessary to utilize a representation of S_{nl} which retains this flexibility. Formulations such as the discrete interaction approximation, although considerable simplifications, retain the inherent physical properties of the nonlinear interaction, thus accounting for their apparent success.

The computer code used to calculate the nonlinear source terms shown in figures 3, 5, 6 and 7 was provided by Donald Resio of the Florida Institute of Technology. His valuable contribution in making this code available is much appreciated. Specific computer code was written to evaluate figure 4 as the loci scaling makes these terms difficult to extract from the full Resio model. Much of the work described has developed as a result of a series of remarkable studies by Klaus Hasselmann. His valuable comments on the paper are gratefully acknowledged.

References

Banner, M. L. 1990 Equilibrium spectra of wind waves. *J. Phys. Oceanogr.* **20**, 966–984.

Barnett, T. P. 1968 One the generation, dissipation and prediction of ocean wind waves. *J. geophys. Res.* **73**, 513–529.

Barnett, T. P. & Sutherland, A. J. 1968 A note on an overshoot effect in wind-generated waves. *J. geophys. Res.* **73**, 6879–6885.

Donelan, M. A., Hamilton, J. & Hui, W. H. 1985 Directional spectra of wind-generated waves. *Phil. Trans. R. Soc. Lond.* A **315**, 509–562.

Dungey, J. C. & Hui, W. H. 1979 Nonlinear energy transfer in a narrow gravity-wave spectrum. *Proc. R. Soc. Lond.* A **368**, 239–265.

Ewing, J. A. 1971 A numerical wave prediction method for the North Atlantic Ocean. *Dtsch. Hydrogh. Z.* **24**, 241–261.

Fox, M. J. H. 1976 On the nonlinear transfer of energy in the peak of a gravity-wave spectrum II. *Proc. R. Soc. Lond.* A **348**, 467–483.

Gelci, R., Cazalé, H. & Vassal, J. 1957 Prévision de la houle. La méthode des densités spectroangulaires. *Bull. Inform. Comité Central Oceanogr. d'Etude Côtes* **9**, 416–435.

Günther, H., Hasselmann, S. & Janssen, P. A. E. M. 1991 *WAMODEL Cycle 4.* Tech. Rep. no. 4, Deutsches Klima Rechen Zentrum, Hamburg, Germany.

Gelci, R. & Chavy, P. 1978 Seven years of numerical wave prediction with the DSA5 model. In *Turbulent fluxes through the sea surface, wave dynamics and prediction* (ed. A. Favre & K. Hasselmann), pp. 565–591. New York: Plenum Press.

Gelci, R. & Devillaz, E. 1970 Le calcul numérique de l'état de la mer. *Houille Blanche* **25**, 117–131.

Hasselmann, D. E., Dunckel, M. & Ewing, J. A. 1980 Directional wave spectra observed during JONSWAP 1973. *J. phys. Oceanogr.* **10**, 1264–1280.

Hasselmann, K. 1960 Grundgleichungen der Seegangsvoraussage. *Schiffstech.* **1**, 191–195.

Hasselmann, K. 1962 On the non-linear energy transfer in a gravity-wave spectrum, part 1. General theory. *J. Fluid Mech.* **12**, 481–500.

Hasselmann, K. 1963*a* On the non-linear energy transfer in a gravity-wave spectrum, Part 2. Conservation theorems; wave-particle analogy; irreversibility. *J. Fluid Mech.* **15**, 273–281.

Hasselmann, K. 1963*b* On the non-linear energy transfer in a gravity-wave spectrum, Part 3. Evaluation of energy flux and swell–sea interaction for a Neumann spectrum. *J. Fluid Mech.* **15**, 385–398.

Hasselmann, K. 1966 Feyman diagrams and interactions rules of wave–wave scattering processes. *Rev. Geophys.* **4**, 1–32.

Hasselmann, K. *et al.* 1973 Measurements of wind-wave growth and swell decay during the Joint North Sea Wave Project (JONSWAP). *Dtsch. Hydrogh. Z.* (*Suppl.*) A **8**, 12.

Hasselmann, S. & Hasselmann, K. 1981 A symmetrical method of computing the nonlinear transfer in a gravity wave spectrum. *Hamburger Geophys. Einzelschriften* A **52**.

Hasselmann, S. & Hasselmann, K. 1985*a* The wave model EXACT-NL. In *Ocean wave modelling* (The SWAMP Group), pp. 249–251. New York: Plenum Press.

Hasselmann, S. & Hasselmann, K. 1985*b* Computations and parameterizations of the nonlinear energy transfer in a gravity-wave spectrum. Part 1: A new method for efficient computations of the exact nonlinear transfer integral. *J. phys. Oceanogr.* **15**, 1369–1377.

Hasselmann, S., Hasselmann, K., Allender, J. H. & Barnett, T. P. 1985 Computations and parameterizations of the nonlinear energy transfer in a gravity-wave spectrum. Part 2: Parameterizations of the nonlinear transfer for application in wave models. *J. phys. Oceanogr.* **15**, 1378–1391.

PHILOSOPHICAL TRANSACTIONS OF THE ROYAL SOCIETY A MATHEMATICAL, PHYSICAL & ENGINEERING SCIENCES

Herterich, K. & Hasselmann, K. 1980 A similarity relation for the nonlinear energy transfer in a finite-depth gravity-wave spectrum. *J. Fluid Mech.* **97**, 215–224.

Holthuijsen, L. H. 1983 Observations of the directional distribution of ocean-wave energy in fetch-limited conditions. *J. phys. Oceanogr.* **13**, 191–207.

Komen, G. J., Hasselmann, S. & Hasselmann, K. 1984 On the existence of a fully developed wind–sea spectrum. *J. phys. Oceanogr.* **14**, 1271–1285.

Longuet-Higgins, M. S. 1976 On the nonlinear transfer of energy in the peak of a gravity-wave spectrum: A simplified model. *Proc. R. Soc. Lond.* A **347**, 311–328.

Masuda, A. 1980 Nonlinear energy transfer between wind waves. *J. phys. Oceanogr.* **10**, 2082–2093.

Mitsuyasu, H. 1975 Observations of the directional spectrum of ocean waves using a cloverleaf buoy. *J. phys. Oceanogr.* **5**, 750–759.

Phillips, O. M. 1960 On the dynamics of unsteady gravity waves of finite amplitude, Part 1. *J. Fluid Mech.* **9**, 193–217.

Phillips, O. M. 1981 Wave interactions – the evolution of an idea. *J. Fluid Mech.* **106**, 215–227.

Pierson, W. J. & Moskowitz, L. 1964 A proposed spectral form for fully developed wind seas based on the similarity theory of S. A. Kitaigorodskii. *J. geophys. Res.* **69**, 5181–5190.

Pierson, W. J., Tick, L. J. & Baer, L. 1966 Computer based procedure for preparing global wave forecasts and wind field analysis capable of using wave data obtained from a spacecraft. In *Proc. Sixth Symp. Naval Hydrodynamics*. Washington, D.C., U.S.A.

Resio, D. & Perrie, W. 1991 A numerical study of nonlinear energy fluxes due to wave–wave interactions. Part 1: Methodology and basic results. *J. Fluid Mech.* **223**, 609–629.

Sell, W. & Hasselmann, K. 1972 *Computations of nonlinear energy transfer for JONSWAP and empirical wind-wave spectra. Report of the Institute of Geophysics, University of Hamburg, Germany.*

SWAMP 1985 *Ocean wave modeling*. New York: Plenum Press.

Tolman, H. L. 1991 A third-generation model for wind waves on slowly varying, unsteady, and inhomogeneous depth and currents. *J. phys. Oceanogr.* **21**, 782–797.

Tracy, B. A. & Resio, D. T. 1982 *Theory and calculation of the nonlinear energy transfer between sea waves in deep water*, Report no. 11, U.S. Army Engineer Waterways Experiment Station, Vicksburg, U.S.A.

Van Vledder, G. Ph. & Weber, S. L. 1988 *Guide for the program EXACT-NL*. Report no. 20, Max-Planck-Institut für Meteorologie, Hamburg, Germany.

Van Vledder, G. Ph. 1990 *Directional response of wind waves to turning winds*. Rep. no. 90–2, Faculty of Civil Engineering, Delft University of Technology, The Netherlands.

Van Vledder, G. Ph. & Holthuijsen, L. H. 1993 The directional response of ocean waves to turning winds. *J. phys. Oceanogr.* **23** (In the press.)

WAMDI 1988 The WAM model – A third generation ocean wave prediction model. *J. phys. Oceanogr.* **18**, 1775–1810.

Webb, D. J. 1978 Non-linear transfers between sea waves. *Deep-Sea Res.* **25**, 279–298.

Weber, S. L. 1988 The energy balance of finite depth gravity waves. *J. geophys. Res.* **93**, C4, 3601–3607.

Willebrand, J. 1975 Energy transport in a nonlinear and inhomogeneous random wave field. *J. Fluid Mech.* **70**, 113–126.

Young, I. R., Hasselmann, S. & Hasselmann, K. 1987 Computations of the response of a wave spectrum to a sudden change in the wind direction. *J. phys. Oceanogr.* **17**, 1317–1338.

Young, I. R. 1988 A shallow water spectral wave model. *J. Geophys. Res.* **93**, 5113–5129.

Zakharov, V. E. & Filonenko, N. N. 1967 Energy spectrum for stochastic oscillations of the surface of a liquid. *Soviet Phys. Dokl.* **11**, 881–883.

Received 21 October 1991; revised 22 April 1992; accepted 6 August 1992

PHILOSOPHICAL TRANSACTIONS OF THE ROYAL SOCIETY A MATHEMATICAL, PHYSICAL & ENGINEERING SCIENCES

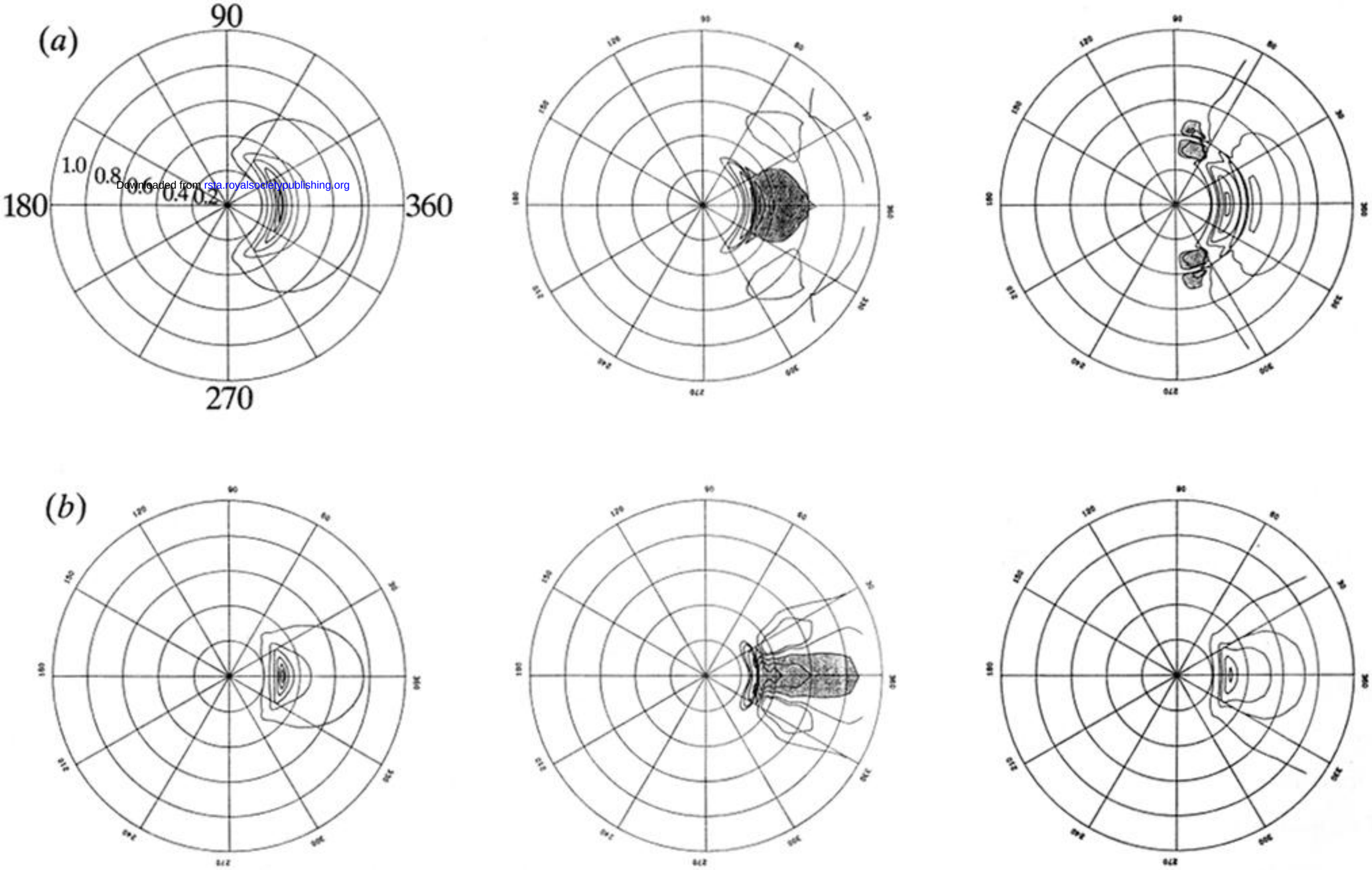

Figure 7. Isoline plots of the spectrum (left), S_{nl} (middle) and S_{tot} (right) for a directional spread of the form (*a*) $\cos^2\theta$ and (*b*) $\cos^{10}\theta$. Spectral contours are drawn at 0.01, 0.1, 0.25, 0.5, 0.75 and 0.9 times the spectral maximum. Contours of S_{nl} are drawn at -0.9, -0.5, -0.2, -0.1, 0.1, 0.2, 0.5 and 0.9 times the maximum positive value of S_{nl} and contours of S_{tot} at -0.05, -0.01, 0.1, 0.2, 0.5 and 0.9 times the maximum positive value of S_{tot}. Negative regions of S_{nl} and S_{tot} are shaded.